





Biomedical Applications of Bisphosphonate Chelating Agents by Metal Cations as Drug Design for Prevention and Treatment of Osteoporosis using QM/MM Method

Fatemeh Mollaamin^{1,*} , Selahattin Özcan² , Esra Özcan³ , Majid Monajjemi⁴ 

¹ Department of Biomedical Engineering, Faculty of Engineering and Architecture, Kastamonu University, Kastamonu, Turkey

² Department of Orthopedics and Traumatology, Faculty of Medicine, Kastamonu University, Kastamonu, Turkey

³ Department of Physical Medicine and Rehabilitation, Faculty of Medicine, Kastamonu University, Kastamonu, Turkey

⁴ Department of Chemical Engineering, Central Tehran Branch, Islamic Azad University, Tehran, Iran

* Correspondence: smollaamin@gmail.com (F.M.);

Scopus Author ID 35848813100

Received: 14.05.2022; Accepted: 21.06.2022; Published: 11.09.2022

Abstract: By investigating their pharmacological activity, bisphosphonate drugs can be employed to prevent the loss of bone density and treat bone diseases like osteoporosis. The capability of bisphosphonates is to be stuck and be kept within bone during osteoclast-mediated bone inorganic material decomposition. The main problem accompanied by their application is their low oral bioavailability. Several delivery systems, such as metal chelating, nanoparticles, and contrast agents, have been selected to modify their absorption and to conduct them to sites other than bone cells. In this contribution, we have investigated the pharmacological and clinical application of bisphosphonate drugs of 5AFX, 4QPF, 3DYG, 2I19, and 2F92 using novel QM/MM applications of DFT, MC, and MD due to physicochemical properties of NMR, charge transfer, Gibbs free energy, electronic-kinetic and nuclear repulse energies in the pharmaceutical and biomedical fields. The bisphosphonate agent has been accomplished in chelation with the metal cation of Mg^{2+} and Cu^{2+} through the PDB structures of 5AFX, 4QPF, 3DYG, 2I19, and 2F92 drugs. Since the metal binding of phosphonate groups is relatively bulky, with six oxygens having a negative charge more than $pH=4$, which is high (approximately four per ligand), these structures are active in forming the chelated compounds through the drug design method. The connection between structure and activity methods play an important role in predicting the biological properties of target compounds and their physicochemical properties. In this article, Ramachandran plot in drug design has played an efficient function in target identification and designing novel drugs for exploring the parameters of amino acid sequence, molecular modeling, and the 3-D structure bisphosphonate agents of novel drugs of 5AFX, 4QPF, 3DYG, 2I19, and 2F92.

Keywords: osteoporosis; bisphosphonate drugs; 5AFX; 4QPF; 3DYG; 2I19; 2F92; chelation; metal cations; Mg^{2+} ; Ca^{2+} ; QM/MM; DFT; NMR; MC.

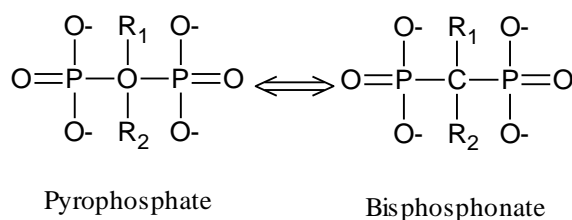
© 2022 by the authors. This article is an open-access article distributed under the terms and conditions of the Creative Commons Attribution (CC BY) license (<https://creativecommons.org/licenses/by/4.0/>).

1. Introduction

Bisphosphonates with two phosphonates $[PO(OH)_2]$ groups are a collection of drugs that keep the bone from the destruction of density, used to prevent and treatment of osteoporosis, malignancy-associated hypercalcemia, fibrous dysplasia, pediatric bone diseases, bone metastases, and other similar diseases [1-5]. In addition, they decrease the conditions

involving fragile, breakable bone and the probability of vertebral fracture in steroid-induced osteoporosis for postmenopausal women [6].

Bisphosphonates are analogs of pyrophosphates that happen physiologically and in which the atom of O in the heart of the P-O-P structure has been substituted by carbon (P-C-P group) (Scheme 1).



Scheme 1. The structure of pyrophosphate and of bisphosphonates.

Further exchanges have synthesized a series of active bisphosphonates with each its characteristic potential activity and effect on bone. Therefore, every bisphosphonate has to be evaluated individually.

The most common bisphosphonate drugs for the treatment of osteoporosis are alendronate, risedronate, intravenous pamidronate, strontium ranelate, or teriparatide which are used for refractory disease [7-13]. The bisphosphonates are divided into chemical groups based on the side chains of R₁ and R₂ (Table 1).

Table 1. The categorization of the bisphosphonate class with R₁, R₂ side chains.

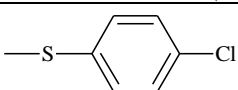
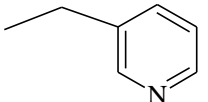
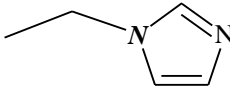
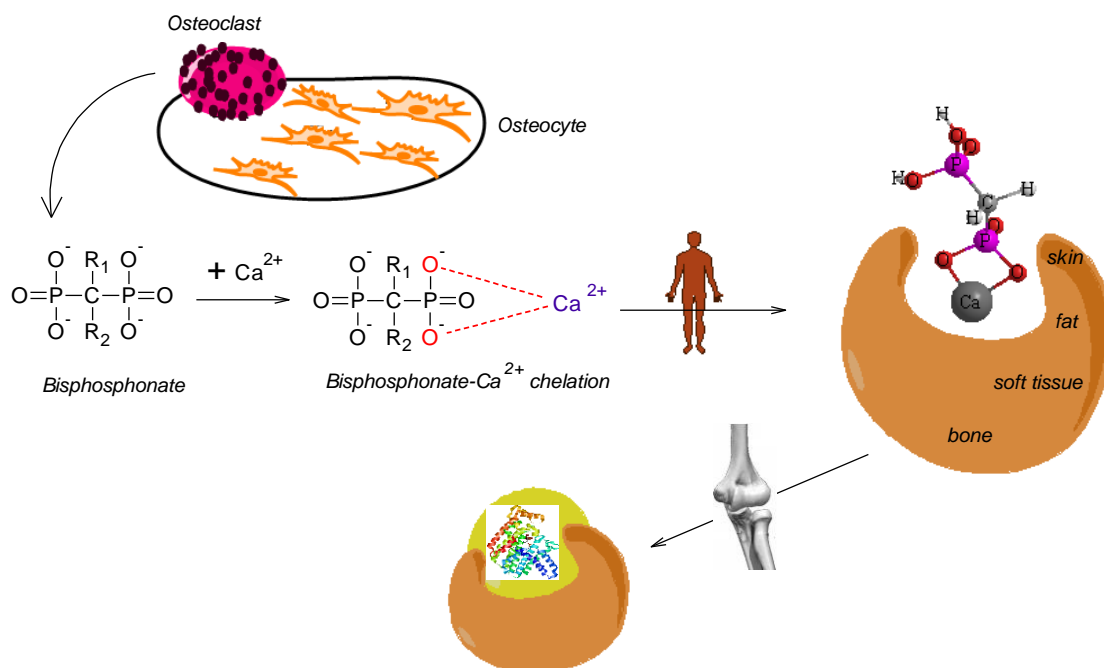
Agent	Side chain of R ₁	Side chain of R ₂	Subdivision into chemical groups
Clodronate	-Cl	-Cl	without nitrogen substitution
Etidronate	-OH	-CH ₃	
Alendronate	-OH	-(CH ₂) ₃ -NH ₂	Aminobisphosphonates
Pamidronate	-OH	-CH ₂ -CH ₂ -NH ₂	
Neridronate	-OH	-(CH ₂) ₅ -NH ₂	
Olpadronate	-OH	-(CH ₂) ₂ -N(CH ₃) ₂	
Ibandronate	-OH	-CH ₂ -CH ₂ N $\begin{array}{l} \diagup \text{CH}_3 \\ \diagdown (\text{CH}_2)_4\text{-CH}_3 \end{array}$	Aminobisphosphonates with substitution of the nitrogen atom
Tiludronate	-H		without nitrogen substitution
Risedronate	-OH		Bisphosphonates with basic heterocycles containing nitrogen
Zoledronate	-OH		

Table 1 shows a central carbon in bisphosphonates with two side chains of R₁, R₂ (with and without nitrogen which acts differently in killing osteoclasts), and two phosphate groups that are binded to calcium cations for saving a high amount of this cation in bones of the human body (Scheme 2).

Osteoclasts (the bone cells that break down bone tissue) release bisphosphonates which are bonded to bone tissue. Then, bisphosphonate molecules are joined to and enter osteoclasts, where they interrupt intracellular enzymatic functions necessary for bone resorbing [14].



Scheme 2. Mechanism of chelating of bisphosphonates to the bone of the human body.

Bone tissue endures fixing remaking and becomes in balance via osteoblasts producing bone and osteoclasts ruining bone. Bisphosphonates prevent the digestion of bone by motivating osteoclasts to endure apoptosis or cell death, which decreases the speed of bone destruction [15].

Bisphosphonates associate at sites of bone destruction by attaching to hydroxyapatite and are selectively entered by actively resorbing osteoclasts. The various bisphosphonates have various tendencies for hydroxyapatite structures. These differences in junction and impacts on mineral superficies attribute such as absorbing and keeping on the skeleton, diffusing the drug within the bone, delivering of absorbed drug from the bone, reusing the ability of the desorbed drug back onto surficial bone, impacting on mineral force power and cellular operators can be presented in the clinical differences between these bisphosphonates.

Bisphosphonates might be prescribed orally as tablets or intravenously as infusions. The sorption of the intestine for new bisphosphonates is minimal to low (<1 to 3 %). Two attributes of bisphosphonates, including their low tendency for lipids which prevent passing through membranes and into the cell, and their polarity, which hinders para-cellular transition, approve their poor absorption. Bisphosphonate sorption decreases by ingesting food (particularly food rich in calcium), like milk and milk products, because they produce insoluble chelates with the calcium in these compounds (Scheme 2).

Different compounds with side chains of R_1 and R_2 of bisphosphonates are bonded to albumin in the blood with a big difference in the strength of the albumin bonds, so, it takes time for them to be separated from the plasma and be joined to the blood.

Skeletal retaining differs with various bisphosphonates, and an important parameter is the speed of bone torsion and the number of superficies of bone. This retaining in bone is identical to that of compounds like strontium, fluoride, and tetracyclines. The long-time superficies linkage of bisphosphonates indicates their expanded time of function. The shortest time for pharmacological impact is observed 24 hours after administrating.

In our body, the bone cells are slowly being constantly taken away and substituted with new bone cells by osteoblasts throughout life. Bisphosphonates decrease osteoclast activity and

therefore decrease the overturn of bone or replacement of old bone. When we age, and in special diseases, the bone is damaged or removed more rapidly than our body can substitute it. This makes the bones weakened, thin, and much easier to break with even a small effect or a fall from a standing height. So, bisphosphonate medications help to keep our bone density and bone strength.

2. Materials and Methods

2.1. Ramachandran plot for bisphosphonate drugs.

The Ramachandran diagram with $[\phi, \psi]$ has indicated the regions for backbone dihedral angles ψ against ϕ of amino acid residues in bisphosphonate drug of 4QPF (Figure 1) energetically.

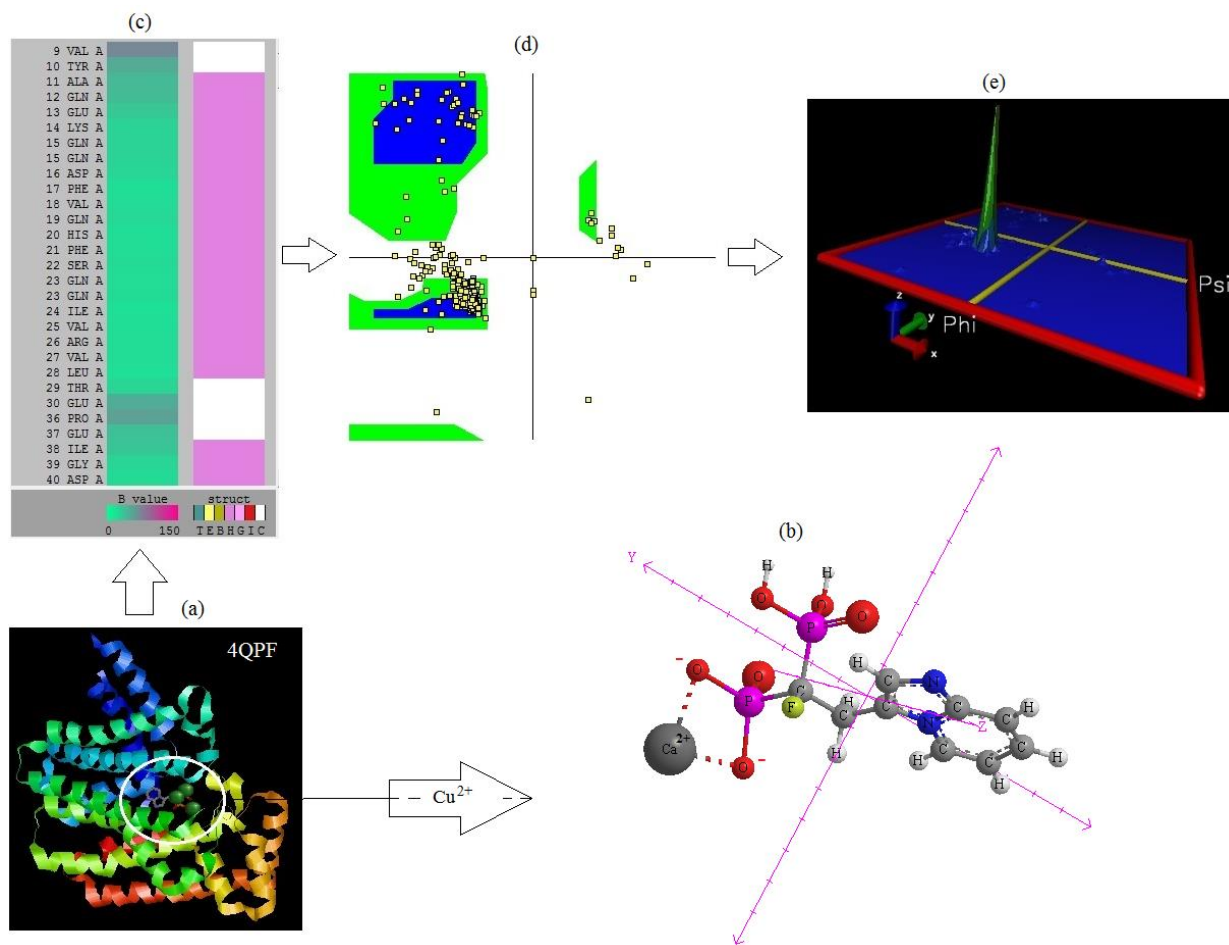


Figure 1. (a) 3-D structure of 4QPF by raswin software as Ribbon view (b) optimized structure of bisphosphonate agent of 4QPF chelated to metal cation of Ca^{2+} , (c) sequence viewer of amino acids, (d) Ramachandran plot, and (e) 3-D histogram of Ramachandran using VMD (1.9.4) program package.

Figure 1a shows shown 3-D structure of 4QPF in ribbon view state from high-resolution protein structures established by X-ray crystallography and deposited in the Protein Data Bank (PDB), which can be chelated with Ca^{2+} due to R_2 side chain (Figure 1b). The sequence viewer in the Ramachandran plot (Figure 1c) has illustrated the data points (yellow points) from a large set of high-resolution structures and contours for favored and for allowed conformational zones for bisphosphonate of 4QPF (Figure 1d). A 3-D Ramachandran plot has been applied to present the conformations of the ψ and ϕ angles (Figure 1e) and the possibility for an amino-

acid residue in the bisphosphonate drug, which indicates the empirical distribution of data points (yellow points) observed in 4QPF.

The Ramachandran plots for four bisphosphonate drugs of 5AFX, 3DYG, 2I19, and 2F92 in Figure 2 have depicted the data points from a large set of high-resolution structures and contours for favored (blue zone), allowed (green zone corresponds to conformations where atoms in the PDB structure come closer than the sum of their van der Waals radii.) and disallowed or outlier region (white zone) conformational regions for these drugs using Visual Molecular Dynamics (VMD 1.9.4) which is a software for molecular modeling and visualization of molecular dynamics simulations (Figure 2) [16].

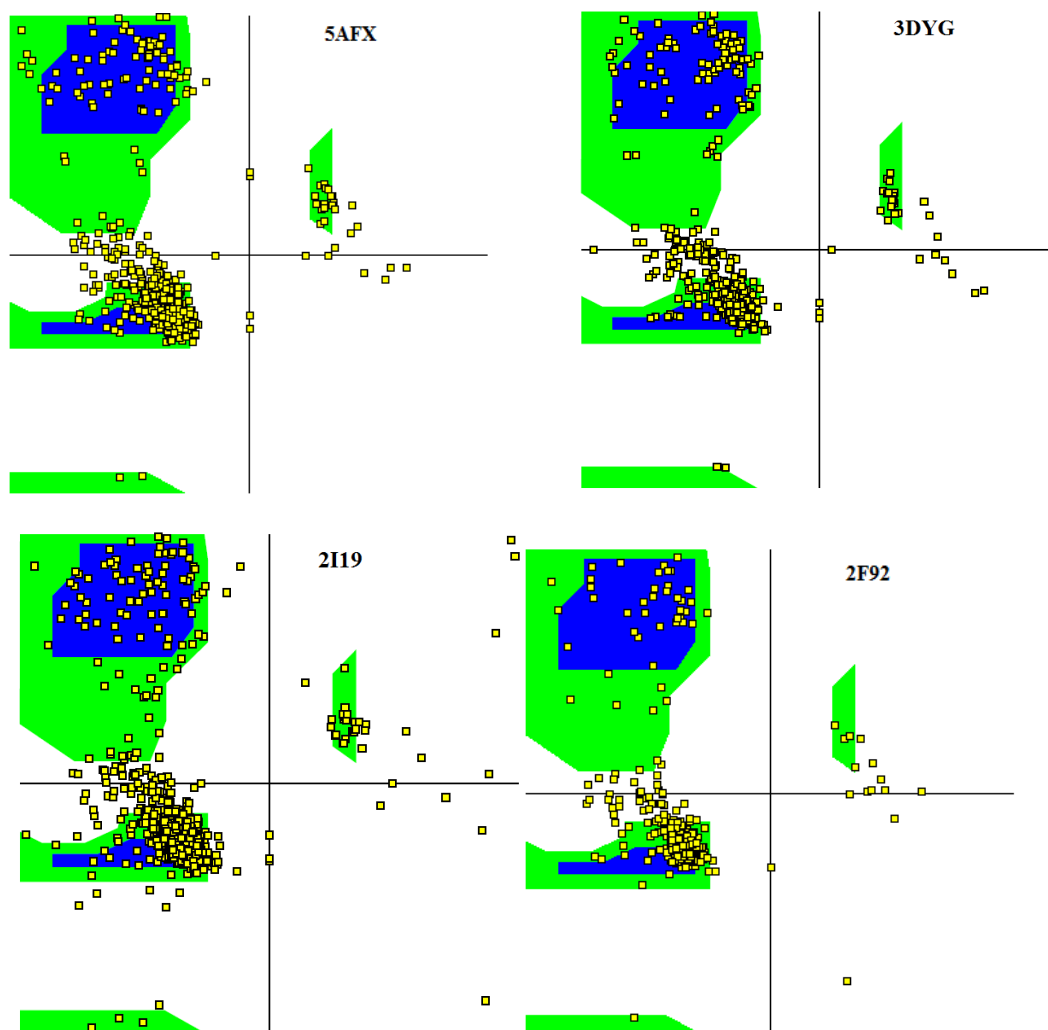


Figure 2. The Ramachandran plots generated from bisphosphonate drugs with PDB ID, including 5AFX, 3DYG, 2I19, and 2F92. The blue, green, and white regions represent the favored, allowed, and disallowed or outlier regions with yellow data points of the amino acid sequence.

The Ramachandran plots for 5AFX, 3DYG, 2I19, and 2F92 in Figure 2 are based on non-bonded interaction statistics between various atom types computed by its precise structure database.

It may be estimated that larger side chains of R₂ in the bisphosphonate drugs of 5AFX, 3DYG, 2I19, and 2F92 (Figure 2) would lead us to more constrictions and follow a smaller permissible zone in the Ramachandran plot. Still, the influence of side chains is lowercase. The main observable influence is the existence or lack of the methylene group. In Figure2, it has been denoted the most allowable zone for 2I19 with a much smaller van der Waals radius than the side chain of all other bisphosphonate drugs. The most diffusion of data points of amino

acids in the favorable and allowable zones is 2I19 > 5AFX ≥ 3DYG > 2F92 ≥ 4QPF, respectively (Figures 1 and 2). These residues of bisphosphonate drugs might be modeled with minimized energy that points out more effective structures due to better stereochemical properties.


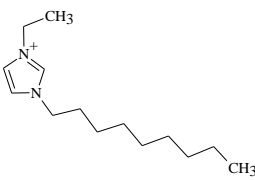

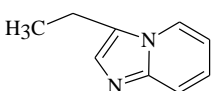
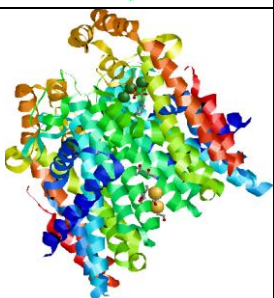
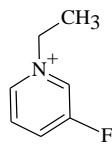
2.2. Theory of bisphosphonate chelating agent with cations.

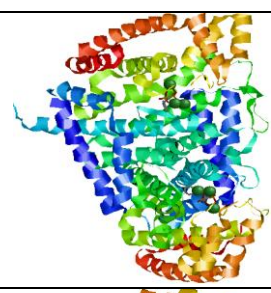
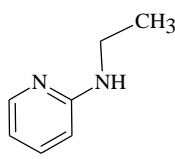
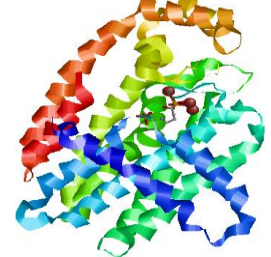
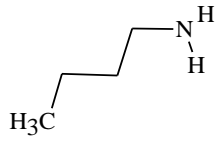
A kind of bonding of ions and molecules to metal ions is chelation which deals with the formation or existence of two or more separate coordinate bonds between a multiple bonded ligand that is called chelating or sequestering agents and a single central metal atom. Chelation can be applied between drugs and metal ions. For instance, antibiotic drugs of the tetracycline and quinolone families are chelating agents of Fe^{2+} , Ca^{2+} , and Mg^{2+} ions [17,18].

The chelation of bisphosphonates with cations in bone cells has been investigated in this work by forming relatively stable complexes. Thus, a series of quantum theoretical approaches have been done to find the optimized coordination of [bisphosphonate----cations of Ca^{2+} and Mg^{2+}] cluster chelation in bone with NMR in the Gaussian09 program package [19].

Table 2 categorizes the PDB structures of 5AFX, 4QPF, 3DYG, 2I19, and 2F92 as the bisphosphonate drugs which have been recommended for preventing the loss of bone density and osteoporosis treatment with the name and formula and two sides chains of R_1 , R_2 using X-RAY method.

Table 2. The new categorization of the bisphosphonate drugs (5AFX, 4QPF, 3DYG, 2I19, 2F92) with R_1 , R_2 side chains based on PDB structure using X-RAY diffraction.

Agent of bisphosphonate drugs	Ribbon view of PDB structure	R_1	R_2	Name to structure formula
5AFX		-OH		[1-HYDROXY-2-(1-NONYL-1H-3-LAMDA~5~-IMIDAZOL-3-YL)ETHANE-1,1-DIYL]BIS(PHOSPHONIC ACID) $\text{C}_{14}\text{H}_{29}\text{N}_2\text{O}_7\text{P}_2$
4QPF		-F		[1-FLUORO-2-(IMIDAZO[1,2-a]PYRIDIN-3-YL)ETHANE-1,1-DIYL]BIS(PHOSPHONIC ACID) $\text{C}_9\text{H}_{11}\text{F N}_2\text{O}_6\text{P}_2$
3DYG		-OH		3-FLUORO-1-(2-HYDROXY-2,2-DIPHENYLPYRIDINIUM $\text{C}_7\text{H}_{11}\text{F N O}_7\text{P}_2$

Agent of bisphosphonate drugs	Ribbon view of PDB structure	R ₁	R ₂	Name to structure formula
2I19		-H		[2-(PYRIDIN-2-YLAMINO)ETHANE-1,1-DIYL]BIS(PHOSPHONIC ACID) C ₇ H ₁₂ N ₂ O ₆ P ₂
2F92		-OH		4-AMINO-1-HYDROXYBUTANE-1,1-DIYLDIPHOSPHONATE C ₄ H ₉ N O ₇ P ₂

Unlike their early ones, a new generation of bisphosphonates such as alendronate, risedronate, ibandronate, pamidronate, and zoledronic acid (Table 1) as the second and third generation of bisphosphonates, includes nitrogen atoms in the side chain of R₂ which can promote osteoclast apoptosis (Table 2). Currently, patients achieve the treatment with more potent nitrogen-containing bisphosphonates than the earlier non-nitrogen-containing bisphosphonates, so this paper has focused more on recent bisphosphonate drugs such as 5AFX, 4QPF, 3DYG, 2I19, and 2F92.

These novel drugs have been employed for a new lower bone tendency for bisphosphonate drug design, efficiently curing diseases identified by abnormal bone resorption (4QPF). The development of selective protein farnesyl transferase (FTase) and protein geranylgeranyl transferase (GGTase) inhibitors as anticancer therapeutic agents has discovered 3DYG, which is more active than current bisphosphonate drugs (Table 2) [20].

2I19 is a solid-state (13)C, (15)N, and (31)P magic-angle sample spinning (MAS) NMR and quantum chemical study of several bisphosphonates as pure compounds and bonded to FPPS for preparing information about side chain and phosphonate backbone protonation states when bound to the enzyme (Table 2) [21].

It has been exhibited the results of 925 potential prenyl synthase inhibitors against *Trypanosoma brucei* farnesyl diphosphate synthase (TbFPPS) and against *T. brucei*, the causative agent of African human trypanosomiasis. 5AFX is one of the most potent compounds lipophilic analogs of the bone resorption drug of the zoledronate family (Table 2) [22].

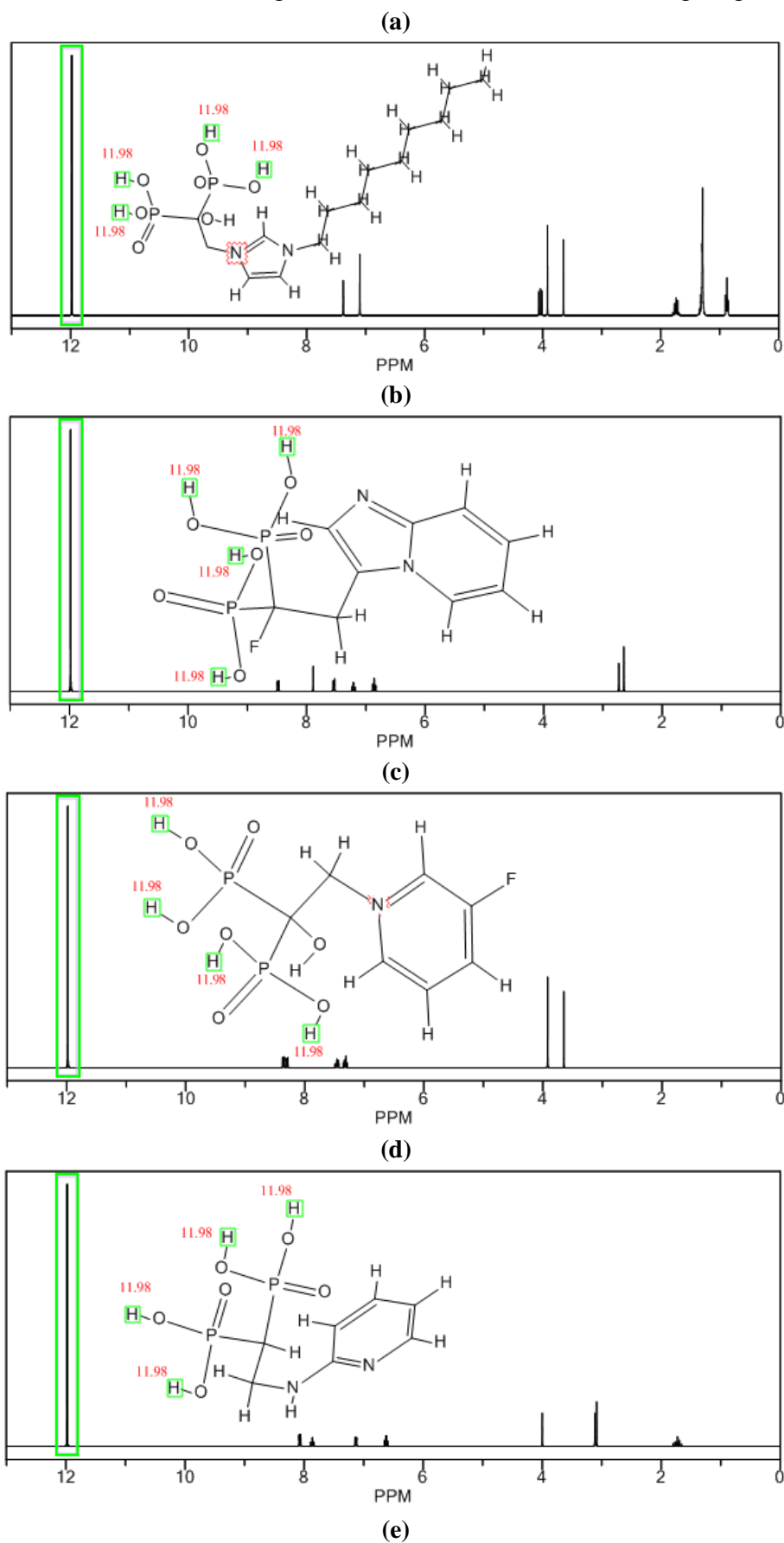
2F92 has been achieved by solving the crystals of human FPPS (farnesyl pyrophosphate synthase) in its unliganded state in a complex with the N-consisting of bisphosphonate (N-BP) medications of alendronate, ibandronate, pamidronate, zoledronate which provide a new accomplishing of the mechanism of FPPS catalysis and inhibition (Table 2) [23].

3. Results and Discussion

3.1. NMR analysis.

¹H-NMR calculations on the active sites of 5AFX, 4QPF, 3DYG, 2I19, and 2F92 chelated to metal cations of Mg²⁺ and Ca²⁺ have been estimated to unravel the indicated atoms

of oxygen in the active sites of these complexes of bisphosphonate as the drugs for osteoporosis and similar diseases treatment through the formation of chelation bonding (Figure 3a-e).



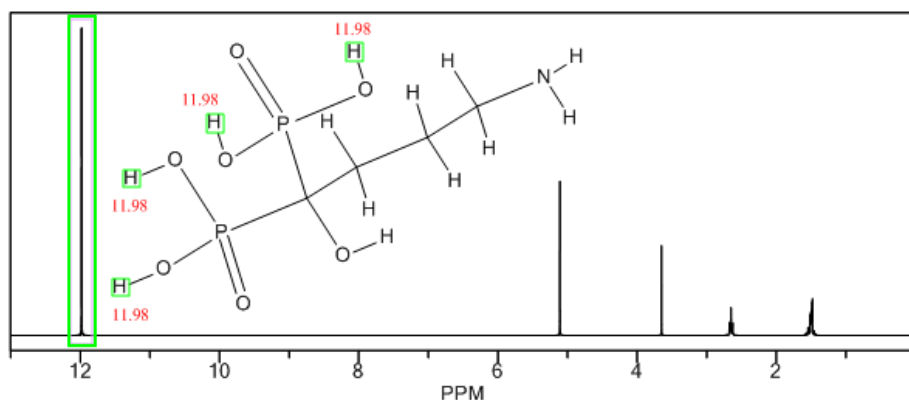


Figure 3. 1H-NMR spectra of (a) 5AFX, (b) 4QPF, (c) 3DYG, (d) 2I19, (e) 2F92 chelated to Mg^{2+} and Ca^{2+} through the drug design method by indicating the active zone of bisphosphonate in the drug design process.

The 1H-NMR measurements demonstrate the active sites of side chains of R_2 (Table 2) of each agent of bisphosphonate drugs, including 5AFX, 4QPF, 3DYG, 2I19, 2F92, while each active atom of oxygen in these compounds as the electronegative atoms for attaching to metal cations of Mg^{2+} and Ca^{2+} denotes the maximal shift in all levels in the NMR spectra; PPM=11.98 for four hydrogens in bisphosphonate agents of 5AFX, 4QPF, 3DYG, 2I19, 2F92 drugs (Figure 3a-e).

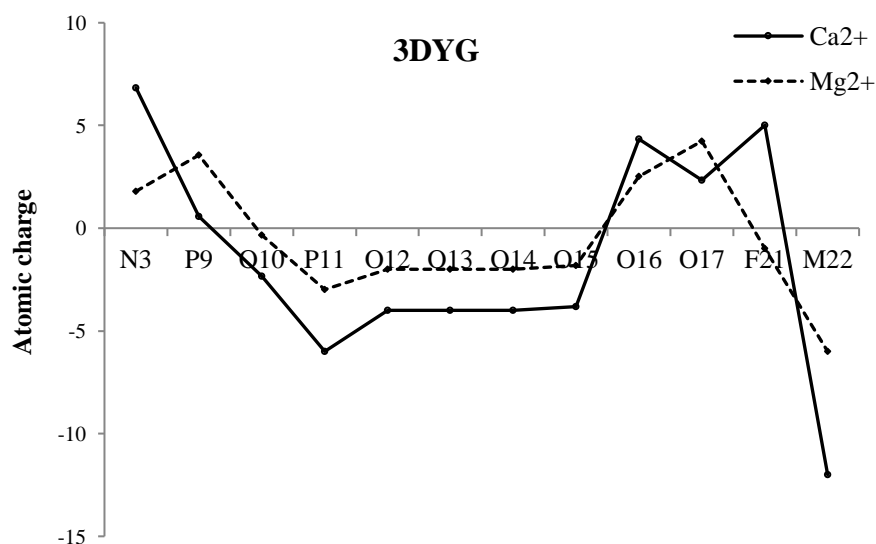
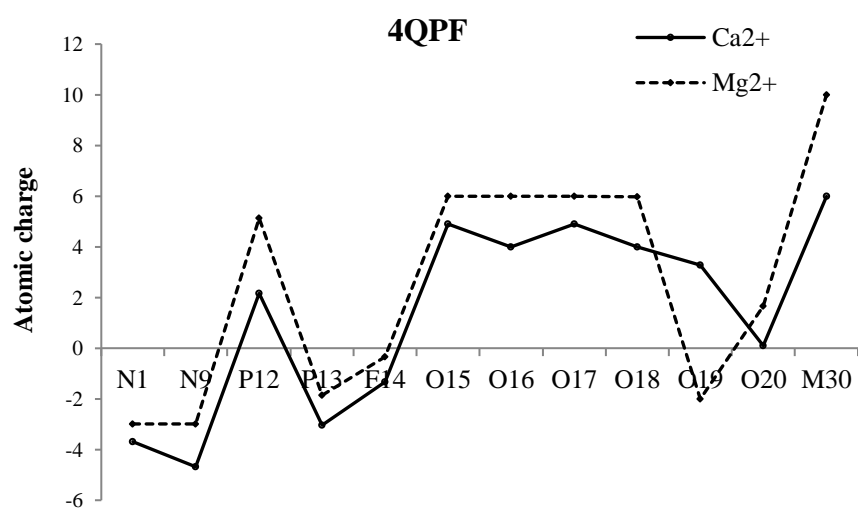
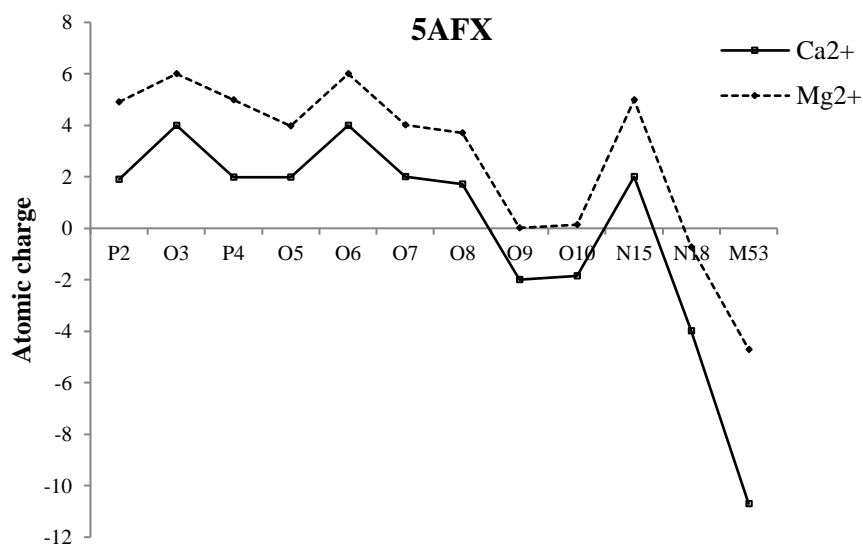
3.2. Charge distribution.

In table 3, the atomic charge of certain atoms in active sites of 5AFX, 4QPF, 3DYG, 2I19, and 2F92 chelated to Mg^{2+} and Ca^{2+} has been evaluated as playing an important role in the electron charge transfer.

Table 3. The atomic charge for nitrogen, phosphorus, oxygen, fluorine, and metallic atoms of magnesium and calcium in molecules of [5AFX, 4QPF, 3DYG, 2I19, 2F92 - Mg^{2+}/Ca^{2+}] complex chelation in water.

Atom	5AFX		Atom	4QPF		Atom	3DYG		Atom	2I19		Atom	2F92	
	Mg^{2+}	Ca^{2+}		Mg^{2+}	Ca^{2+}		Mg^{2+}	Ca^{2+}		Mg^{2+}	Ca^{2+}		Mg^{2+}	Ca^{2+}
P2	4.91	-3.00	N1	-2.99	-0.69	N3	1.78	5.06	N1	-2.00	5.12	P2	3.84	5.06
O3	6.00	-2.00	N9	-2.99	-1.69	P9	3.56	-3.00	N11	-3.00	4.16	O3	-2.00	0.22
P4	4.99	-3.00	P12	5.14	-2.98	O10	-0.33	-2.00	P14	4.97	-3.13	P4	2.77	-2.91
O5	3.98	-2.00	P13	-1.85	-1.19	P11	-2.99	-3.00	P15	-1.08	-3.00	O5	-1.63	-2.00
O6	6.00	-2.00	F14	-0.34	-0.99	O12	-2.00	-2.00	O16	4.03	-2.00	O6	5.97	-2.00
O7	4.01	-2.00	O15	6.00	-1.10	O13	-2.00	-2.00	O17	3.97	-2.00	O7	4.14	3.91
O8	3.71	-2.00	O16	6.00	-2.00	O14	-2.00	-2.00	O18	-2.00	-2.00	O8	4.69	6.00
O9	0.01	-2.00	O17	6.00	-1.10	O15	-1.83	-2.00	O19	4.02	-1.99	O9	5.98	6.00
O10	0.15	-2.00	O18	5.98	-1.99	O16	2.51	1.82	O20	6.01	3.91	O10	1.06	6.00
N15	5.00	-3.00	O19	-2.00	5.27	O17	4.24	-1.9	O21	6.00	-2.00	N17	-3.00	-0.1
N18	-0.73	-3.26	O20	1.66	-1.56	F21	-0.99	6.00	M24	8.02	-6.00	M26	1.78	-5.99
M53	-4.70	-6.00	M30	10.00	-4.01	M22	-6.00	-6.00						

In Figure 4, it has been plotted the changes in atomic charge of labeled nitrogen, phosphorus, oxygen, fluorine, and metallic atoms of magnesium and calcium through optimized [5AFX, 4QPF, 3DYG, 2I19, 2F92 - Mg^{2+}/Ca^{2+}] complexes. So, the results of table 2 in a polar medium of water solution declare the stability of these compounds in the human bone cells for the treatment of osteoporosis.



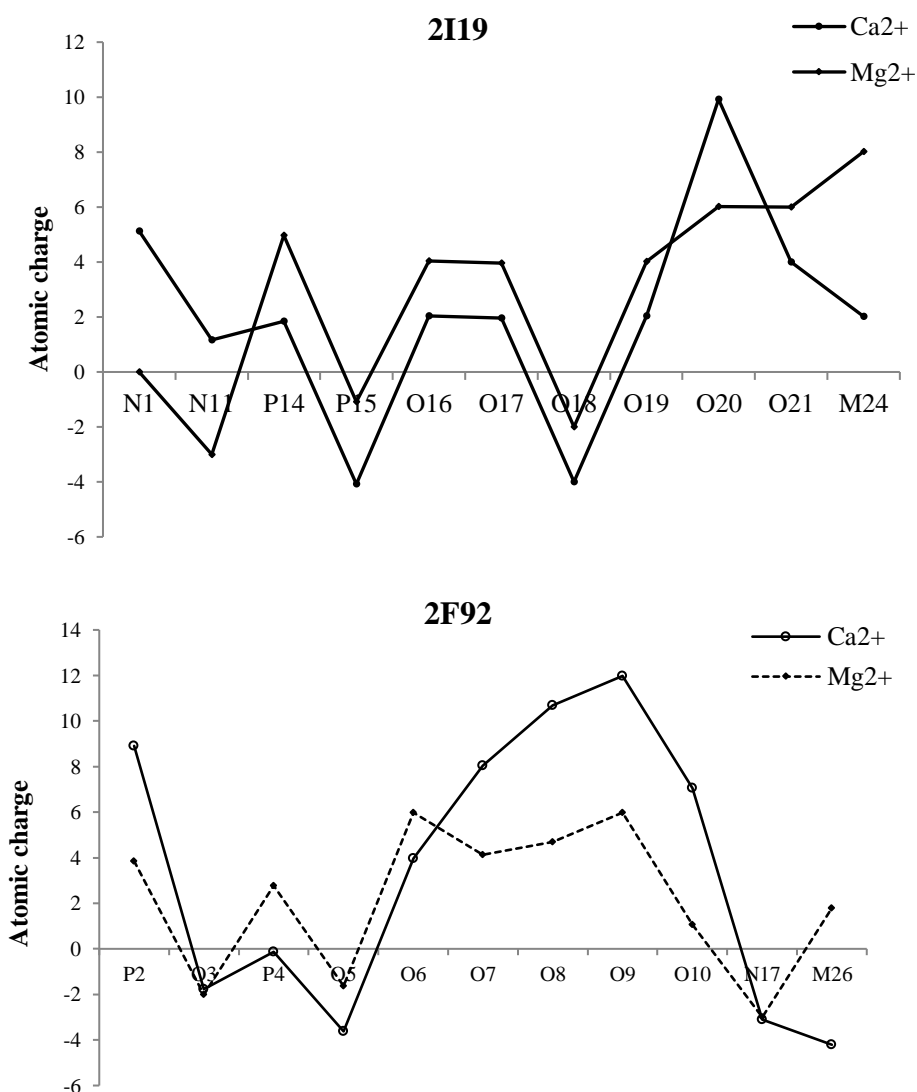


Figure 4. Changes of atomic charge versus labeled nitrogen, phosphorus, oxygen, fluorine, and metal cations through optimized [5AFX, 4QPF, 3DYG, 2I19, 2F92 - Mg²⁺/ Ca²⁺] complex chelation in water medium.

The perspective of Figure 4 recommends the reason for existing observed various results of [5AFX, 4QPF, 3DYG, 2I19, 2F92 - Mg²⁺/ Ca²⁺] complex chelation, which are principally bonded to the position of active sites of labeled nitrogen, phosphorus, oxygen, fluorine, and metallic atoms of magnesium and calcium in five structures which move the charge of electrons in polar bisphosphonates and water molecules.

The partial charges have been obtained by fitting the electrostatic potential to a fixed charge of oxygen atoms of bisphosphonate chelated to cations due to [5AFX, 4QPF, 3DYG, 2I19, 2F92 - Mg²⁺/ Ca²⁺] complexes. Therefore, the electrophilic side chains of 5AFX, 4QPF, 3DYG, 2I19, and 2F92 conduct us to find the reason for the activity and the stability of these structures, which prevent the loss of bone density.

3.3. Physico-chemical analysis using QM/MM method.

Therefore, the physicochemical properties of dipole moment, Gibbs free energy, electronic-kinetic and nuclear repulse energies have determined the stability of bisphosphonate agents among 5AFX, 4QPF, 3DYG, 2I19, 2F92 as the drugs for preventing the loss of bone cells, treatment osteoporosis and other related diseases through the chelated bonding of these

compounds with metal cations of Mg^{2+} and Ca^{2+} using the drug design method (Table 4 and Figure 5a&b).

Table 4. Physico-chemical properties of chelated agents of 5AFX, 4QPF, 3DYG, 2I19, and 2F92 with metal cations of Mg^{2+} and Ca^{2+} at 300 K.

Agent	Metal cation	Gibbs free energy $\times 10^{-4}$ (kcal/mol)	$E_{\text{electronic-kinetic}} \times 10^{-4}$ (kcal/mol)	$E_{\text{nuclear repulsion}} \times 10^{-4}$ (kcal/mol)	Dipole moment (Debye)
5AFX	Mg^{2+}	-98.3810	128.1543	189.9183	2267.8469
	Ca^{2+}	-125.3981	158.0300	199.0882	2324.3960
4QPF	Mg^{2+}	-112.0067	114.3417	139.2580	1010.3054
	Ca^{2+}	-143.1310	147.2889	146.8782	400.0723
3DYG	Mg^{2+}	-109.9116	113.6707	-235.1720	219.9404
	Ca^{2+}	-128.6734	143.9328	132.5761	866.5199
2I19	Mg^{2+}	-954.038	104.7628	120.4234	840.6712
	Ca^{2+}	-119.3344	136.3243	131.9956	476.7009
2F92	Mg^{2+}	-93.4191	98.9178	95.0508	597.7957
	Ca^{2+}	-127.9327	129.1926	102.2586	502.8543

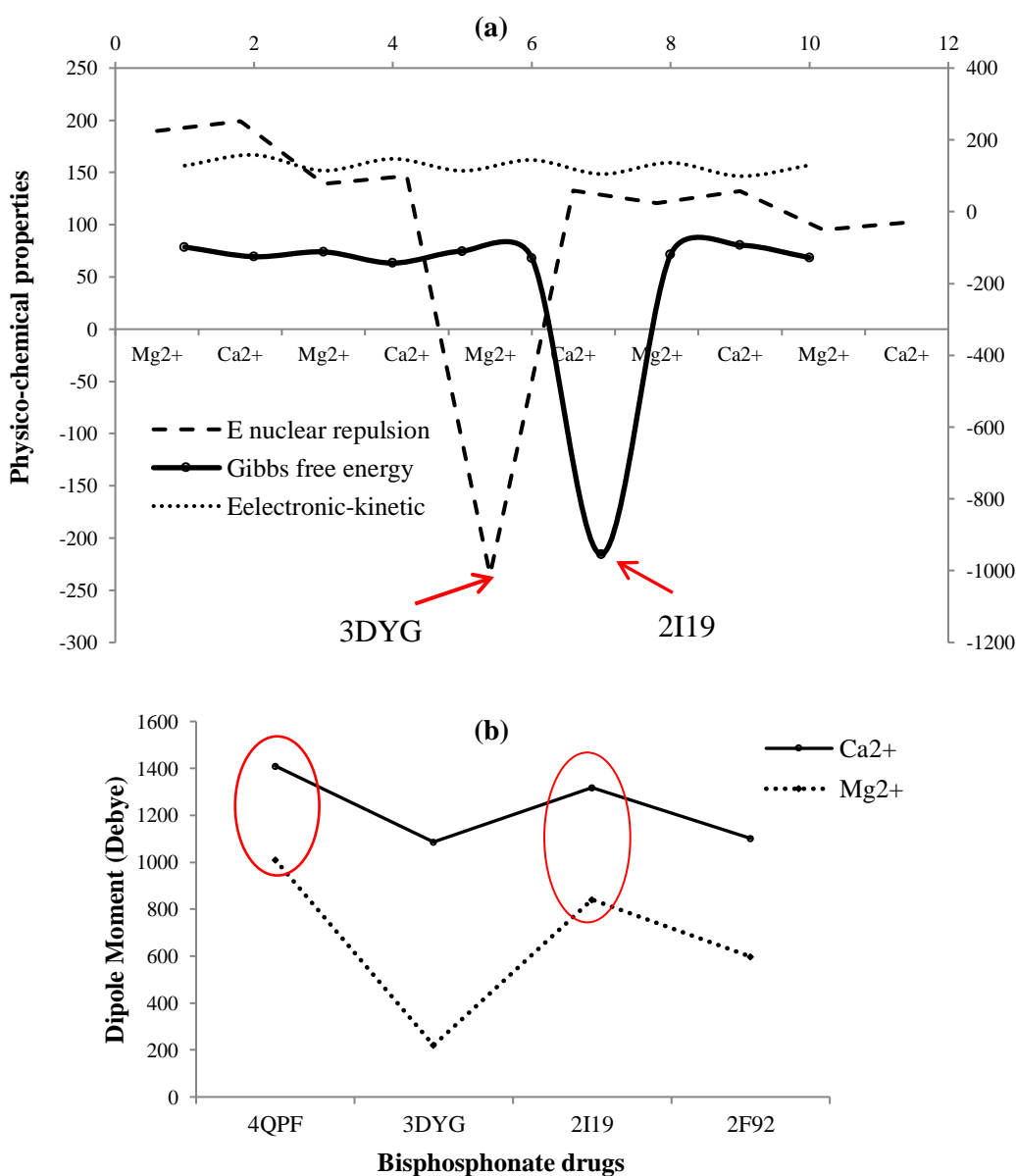


Figure 5. Changes in physicochemical properties of (a) Gibbs free energy, electronic-kinetic, and nuclear repulse energies of bisphosphonate agents among 5AFX, 4QPF, 3DYG, 2I19, 2F92 as the drugs due to the chelated bonding of these compounds with Mg^{2+} and Ca^{2+} metal cations. (b) Dipole moment (Debye) for 5AFX, 4QPF, 3DYG, 2I19, 2F92 chelated to Mg^{2+} and Ca^{2+} for evaluating the polarizability of these selected bisphosphonate drugs.

Figure 5a&b has illustrated the physicochemical parameters related to the biological activity of identified bisphosphonates, including 5AFX, 4QPF, 3DYG, 2I19, 2F92 chelated with Mg^{2+} and Ca^{2+} metal cations have been determined. The main goal of this work was to discover and bring forth molecular recognitions that influence the bioavailability of the above-mentioned compounds as drugs for osteoporosis prevention and treatment. These recognitions are stability of energy, the energy of electronic-kinetic, energy of nuclear-repulsion, as well as dipole moment (Figure 5 a&b). The calculated properties describe solubility and permeability for selected bisphosphonates through biological membranes, which appear as efficient bioavailability indicators of investigated bisphosphonates which can be a sufficient methodology.

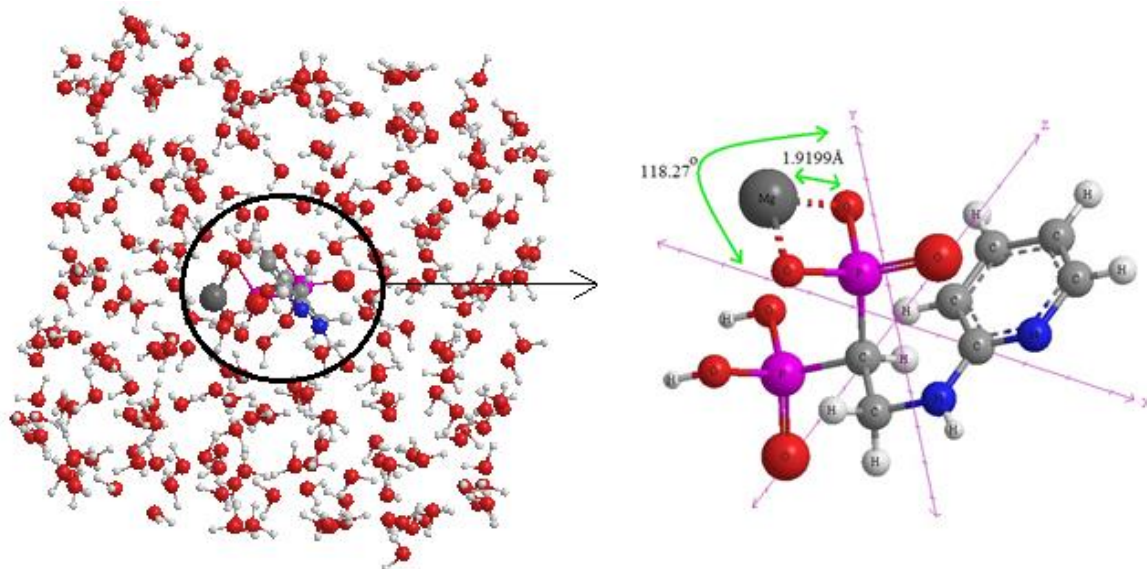
The six atoms of oxygen in each site of the bisphosphonate agents (Scheme 1&2) chelated to metal cations of Mg^{2+} and Ca^{2+} in 5AFX, 4QPF, 3DYG, 2I19, 2F92 drugs have been minimized by an *ab-initio* method using DFT level which includes ECP calculations with theoretical levels of lanl1, lanl2 basis sets and pseudo key for the metal elements. Moreover, these compounds have been predicted by the quantum mechanics and molecular mechanics (QM/MM) method via an ONIOM level. In this investigation, various theoretical commutations have been accomplished towards comparing optimized energies and density diffusions with two approaches of AMBER and OPLS force fields of MM level applying Monte Carlo (MC) and molecular dynamic (MD) optimization. Besides, a professional HyperChem 8 program package [24] has been applied for some extra keywords like PM6 and PM3MM, pseudo=lanl2.

DFT with the van der Waals densities functions had been discussed using modeling of solvent dielectric effects. All calculations of solvent interactions have been achieved by the Gaussian09 package. The data has been computed using the theoretical steps of m062x, m06-L, and m06 for the chelation of bisphosphonate agents-metal cation complexes. The m062x, m06-L, and m06- HF levels have an appropriate correlation in non-bonded computations among solvent and solute. The ONIOM theoretical levels have been accomplished due to three levels of high (H), medium (M), and low (L) calculations which the DFT method has been utilized for the high layer, and the semi-empirical method of PM6 and PM3MM has been exploited for the medium and finally MC for low layers, respectively.

In this research, the polarizable continuum model (PCM) has been used, which is the most popular SCRF model based on apparent surface charges diffusing to non-electrostatic effects with scaled point theory [25,26]. Kirkwood developed the most common levels of the SCRF model of multiple expansions with an algorithm based on applying a strict multipolar expansion up to the seventh order by Frisch that is currently accessible at semi-empirical and *ab initio* levels of theory [27, 28]. Onsager and Kirkwood have arranged an intention for different continuum solvation samples of a multiple expansion (MPE) of the solute charge distribution [29, 30]. Afterward, Wiberg and co-workers developed Onsager-SCRF for the Gaussian program [31]. Solvation is discussed in terms of a dipole moment with an iterative path of quantum mechanics calculations on the compound. The dielectric continuum models, like the self-consistent reaction field methodology, are sufficient in considering the long range of solute-solvent electrostatic interactions and the influence of solvent polarization. Another theoretical level is a combination of molecular mechanics (MM) solvent molecule with quantum mechanics level (QM) for the electronic structure of the solute molecule named QM/MM, which can modify the deficiency of the dielectric continuum model [32,33]. This

investigation has applied the QM/MM method for bisphosphonate drugs of 5AFX, 4QPF, 3DYG, 2I19, and 2F92 chelated to metal cations of Mg^{2+} and Ca^{2+} in a water medium.

So, Hyperchem program software has modeled a water medium for bisphosphonate drugs of 5AFX, 4QPF, 3DYG, 2I19, and 2F92 chelated to metal cations of Mg^{2+} and Ca^{2+} using a periodic box of H_2O molecules via various dimensions. The volume (V) of each box has been yielded by multiple of $V = a \times b \times c$ with the smallest box enclosing solute (Å) including $X \approx 5.5385$, $Y \approx 4.3766$, and $Z \approx 9.4774$, periodic box size of 18.95492 Å, the maximum number of water molecules = 225 and maximum distance between solvents and solute atoms = 2.3 Å for these compounds as the bisphosphonate group of drugs (Scheme 3).



Scheme 3. The schematics of ab initio optimized coordination of 2I19- Mg^{2+} complex through representing the bond length of $\text{O}^- \cdots \text{Mg}^{2+} = 1.9199 \text{ Å}$ and bond angle of $\text{O}^- \cdots \text{Mg}^{2+} \cdots \text{O}^- = 118.27^\circ$ calculated by m062x/cc-pvdz pseudo=lanl2 using QM/MM model in a periodic box of water medium.

The average amount of optimized coordination for bisphosphonate drugs of 5AFX, 4QPF, 3DYG, 2I19, and 2F92 chelated to metal cations of Mg^{2+} and Ca^{2+} has been achieved as the optimized bond length of $\text{O}^- \cdots \text{Mg}^{2+}$ and $\text{O}^- \cdots \text{Ca}^{2+}$, 1.9982 Å and 2.3831 Å; the optimized bond angle of $\text{O}^- \cdots \text{Mg}^{2+} \cdots \text{O}^-$ and $\text{O}^- \cdots \text{Ca}^{2+} \cdots \text{O}^-$, 101.739° and 85.1669°, respectively. In other words, some parameters, like interacting neighboring residues and the atoms involved along with the placement of residues, need to be discussed during the estimation of the validity of a model. In addition, the stereochemical properties of the model, including bond angles, bond lengths, proper chirality, and ring structure coupled with other geometric parameters, need to be evaluated.

3.4. Monte Carlo simulation.

In PDB structure, it can be seen that amines with a chiral carbon directly bonded to the nitrogen are applied due to their vast availability and their strong force on the structure. The chirality within some or all of the individual residues would be needed to direct the formation of a chiral helix because a helix should be chiral. So, molecular mechanics (MM) calculations can estimate the helical structure of PDB structures. In this research, Monte Carlo (MC) simulation has been accomplished on 5AFX, 4QPF, 3DYG, 2I19, and 2F92 chelated to metal cations of Mg^{2+} and Ca^{2+} at 300K energy via time scale (0-100) with max delta and time steps of 0.05 Å, 1, respectively. Optimal values are close to 0.5. Differencing the step size can have

a large influence on the acceptance ratio. The MC options dialog box lets us arrange the MC simulation parameters with 100 steps (Figure 6).

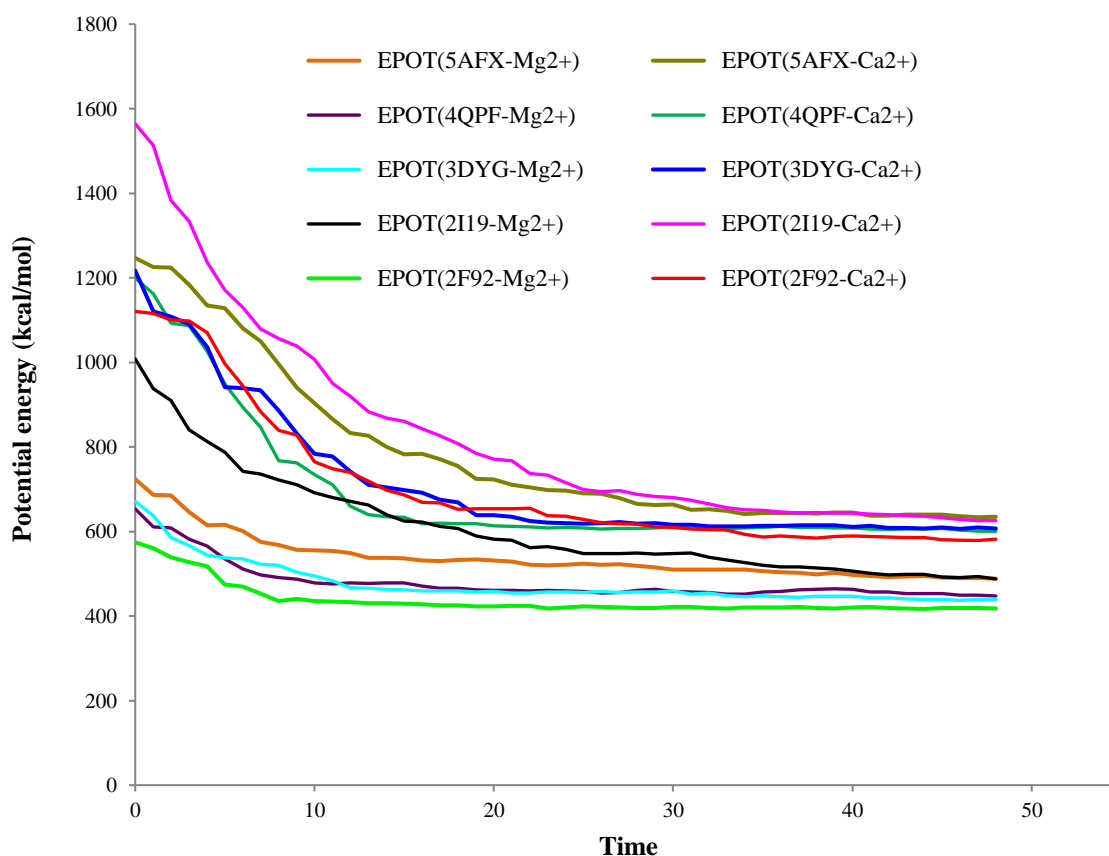


Figure 6. The simulated potential energy of 5AFX, 4QPF, 3DYG, 2I19, and 2F92 chelated to metal cations of Mg^{2+} and Ca^{2+} as the bisphosphonate drugs.

It has been evaluated the possibility of bisphosphonate drugs of 5AFX, 4QPF, 3DYG, 2I19, and 2F92 chelated to metal cations of Mg^{2+} and Ca^{2+} with a simulated model of solute-solvent in a periodic box with a maximum number of water molecules, the minimum distance between solvent and solute molecules using program package HyperChem 8 [34-37]. It has been shown the potential energy graph of [5AFX, 4QPF, 3DYG, 2I19, 2F92 - $\text{Mg}^{2+}/\text{Ca}^{2+}$] chelated complexes in solvent via time scale (0-100) in 300 K using MC method (Max delta = 0.05 Å, time steps=1).

The results of the above observations strongly suggest that the different data observed of 5AFX, 4QPF, 3DYG, 2I19, and 2F92 in the solvent is predominantly due to basis set functions persuaded by a shift in the polarization of the ambient. It is vivid that growth in the dielectric constants augments the resistance and efficiency of these bisphosphonate drugs for preventing the loss of bone density and osteoporosis treatment.

3.5. Molecular dynamic force field.

MD or Molecular dynamic simulation methods forecast how each atom in a protein or other molecular structures can move in the time scale based on a basic physics model through interatomic interactions.

MD consists of conformation studies, thermodynamic factors, and movement instructions of the molecular mechanics and kinetic energy to the potential energy surface. MD simulation evaluates the future speeds and situations of atoms based on their current speeds

and situations. The simulation stimulates the force on each atom (F_i) as the time function through a negative gradient of the potential energy:

$$F_i = -\partial V / \partial r_i \quad (1)$$

where V is the potential energy function, and r_i is the position of atom i . It can be found the acceleration (a_i) of an atom by considering the force action on it by the atom mass:

$$a_i = F_i / m_i \quad (2)$$

The variety of velocities (v_i) is the integral of acceleration over time. The variation in the position (r_i) is the integral of speed over time. Kinetic energy (K) is measured as the speeds of the atoms [38]:

$$K = 1/2 \sum_{i=1}^N m_i v_i^2 \quad (3)$$

The amount of total energy of the Hamiltonian system is the summation of the kinetic and potential energies:

$$H(r, p) = K(p) + V(r) \quad (4)$$

where r is the set of Cartesian coordinates and p is the momenta of the atoms [38,39].

The molecular dynamics method produces a series of time-correlated points in phase space in propagating a starting set of coordinates and speeds according to Newton's second equation by a series of certain time steps. Unlike single point and geometry optimization calculations, molecular dynamics calculation is accounted for thermal motion due to kinetic and potential energy. This work has described in practical terms the types of information MD simulations for bisphosphonate drugs of 5AFX, 4QPF, 3DYG, 2I19, and 2F92 chelated with metal cations of Mg^{2+} and Ca^{2+} at 300 K (Table 5).

Table 5. Molecular dynamic properties of bisphosphonate chelated agents of 5AFX, 4QPF, 3DYG, 2I19, and 2F92 with metal cations of Mg^{2+} and Ca^{2+} at 300 K.

Agent	Metal cation	Potential (kcal/mol)	Kinetic energy (kcal/mol)
5AFX	Mg^{2+}	449.807	29.0368
	Ca^{2+}	630.183	37.4792
4QPF	Mg^{2+}	432.873	17.5323
	Ca^{2+}	419.678	16.1815
3DYG	Mg^{2+}	411.443	10.0416
	Ca^{2+}	578.414	12.1883
2I19	Mg^{2+}	424.738	34.21
	Ca^{2+}	591.041	20.82
2F92	Mg^{2+}	411.074	9.9054
	Ca^{2+}	574.285	13.9996

The spectral pattern of kinetic energy for 5AFX, 4QPF, 3DYG, 2I19, and 2F92 with metal cations of Mg^{2+} and Ca^{2+} at 300 K, and kinetic & potential energy for chelated 5AFX- Cu^{2+} have been evaluated using molecular dynamic method (Figure 7 a&b).

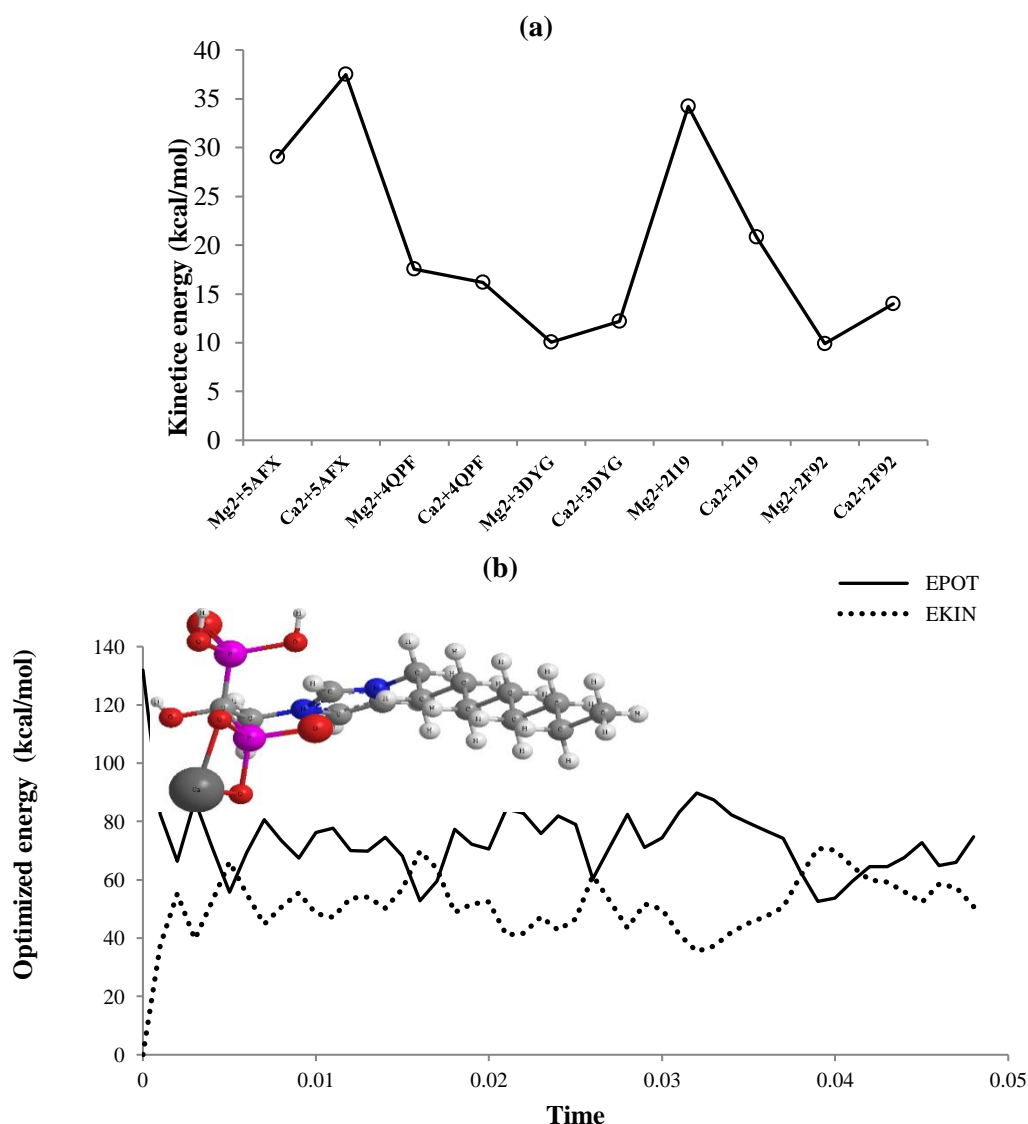


Figure 7. Optimized (a) kinetic energy of 5AFX, 4QPF, 3DYG, 2I19, 2F92 with metal cations of Mg^{2+} and Ca^{2+} at 300 K, (b) kinetic and potential energy for chelated 5AFX- Cu^{2+} by molecular dynamic simulation method.

The control patterns of these complexes were characterized by mechanics data, including RunTime=1 ps, Simulation Temperature=300K and Time Step=0.001 ps.

MD Simulation methods can be trustable in the functional mechanisms of proteins and other biomolecules for unraveling diseases' basic structure and designing and optimizing small molecules, peptides, and proteins.

4. Conclusions

Bisphosphonates have changed the clinical treatment of some skeletal diseases depicted by increasing osteoclast-mediated bone resorption. Molecular modeling structures data quality with the Ramachandran plot, which spreads out, and more residues are likely to be found in the favored regions.

Ramachandran plot has shown the most diffusion of data points of amino acids in the favorable and allowable regions is $2I19 > 5AFX \geq 3DYG > 2F92 \geq 4QPF$, respectively. These residues of bisphosphonate drugs might be simulated with optimized energy, which denotes more sufficient compounds due to better stereochemical parameters.

It has been investigated that [5AFX, 4QPF, 3DYG, 2I19, 2F92 - $\text{Mg}^{2+}/\text{Ca}^{2+}$] chelated complexes are founded on the axes of active parts of identified six oxygens in bisphosphonate agents in PDB structures of 5AFX, 4QPF, 3DYG, 2I19, 2F92 using QM/MM method through 1H-NMR analysis which has highlighted the active site in R₂ side chain in chelating with Mg^{2+} and Ca^{2+} cations.

Moreover, the results of MC and MD calculations on 5AFX, 4QPF, 3DYG, 2I19, and 2F92 have approved the stability and efficiency of these bisphosphonate drugs in different dielectric constants by inducing the change in polarity of ambient.

Funding

This research received no external funding.

Acknowledgments

We thank our colleagues who provided insight and expertise that greatly assisted the research. We would also like to extend our thanks to the Department of Orthopedics and Traumatology and the Department of Physical Medicine and Rehabilitation from the Faculty of Medicine at Kastamonu University.

Conflicts of Interest

The authors declare no conflict of interest.

References

1. Bourrion, B.; Souty, C.; Fournier, L.; Vilcu, A.-M.; Blanchon, T.; Böelle, P.-Y.; Hanslik, T.; François, M. Bisphosphonate Use and Hospitalization for Hip Fractures in Women: An Observational Population-Based Study in France. *Int. J. Environ. Res. Public Health* **2021**, *18*, 8780, <https://doi.org/10.3390/ijerph18168780>.
2. Wu, M.-H.; Lin, Y.-S.; Wu, C.; Lee, C.-Y.; Chen, Y.-C.; Huang, T.-J.; Cheng, J.-S. Timing of Bisphosphonate (Alendronate) Initiation after Surgery for Fragility Fracture: A Population-Based Cohort Study. *J. Clin. Med.* **2021**, *10*, 2541, <https://doi.org/10.3390/jcm10122541>.
3. Montoya-García, M.-J.; Giner, M.; Marcos, R.; García-Romero, D.; Olmo-Montes, F.-J.; Miranda, M.J.; Hernández-Cruz, B.; Colmenero, M.-A.; Vázquez-Gámez, M.A. Fragility Fractures and Imminent Fracture Risk in the Spanish Population: A Retrospective Observational Cohort Study. *J. Clin. Med.* **2021**, *10*, 1082, <https://doi.org/10.3390/jcm10051082>.
4. Li, L.; Yu, M.; Li, Y.; Li, Q.; Yang, H.; Zheng, M.; Han, Y.; Lu, D.; Lu, S.; Gui, L. Synergistic anti-inflammatory and osteogenic n-HA/resveratrol/chitosan composite microspheres for osteoporotic bone regeneration. *Bioact. Mater.* **2021**, *6*, 1255-1266, <https://doi.org/10.1016/j.bioactmat.2020.10.018>.
5. Di Bari, F.; Catalano, A.; Bellone, F.; Martino, G.; Benvenga, S. Vitamin D, Bone Metabolism, and Fracture Risk in Polycystic Ovary Syndrome. *Metabolites* **2021**, *11*, 116, <https://doi.org/10.3390/metabo11020116>.
6. Catalano, A.; Bellone, F.; Santoro, D.; Schwarz, P.; Gaudio, A.; Basile, G.; Sottile, M.C.; Stoian, S.A.; Corica, F.; Morabito, N. Vitamin D Boosts Alendronate Tail Effect on Bone Mineral Density in Postmenopausal Women with Osteoporosis. *Nutrients* **2021**, *13*, 1878, <https://doi.org/10.3390/nu13061878>.
7. Mbese, Z.; Aderibigbe, B.A. Bisphosphonate-Based Conjugates and Derivatives as Potential Therapeutic Agents in Osteoporosis, Bone Cancer and Metastatic Bone Cancer. *Int. J. Mol. Sci.* **2021**, *22*, 6869, <https://doi.org/10.3390/ijms22136869>.
8. Rauner, M.; Taipaleenmäki, H.; Tsourdi, E.; Winter, E.M. Osteoporosis Treatment with Anti-Sclerostin Antibodies-Mechanisms of Action and Clinical Application. *J. Clin. Med.* **2021**, *10*, 787, <https://doi.org/10.3390/jcm10040787>.
9. Geiger, I.; Kammerlander, C.; Höfer, C.; Volland, R.; Trinemeier, J.; Henschelchen, M.; Friess, T.; FLS-CARE study group; Böcker, W.; Sundmacher, L. Implementation of an integrated care programme to avoid fragility fractures of the hip in older adults in 18 Bavarian hospitals—study protocol for the cluster-

- randomised controlled fracture liaison service FLS-CARE. *BMC Geriatr.* **2021**, *21*, 43, <https://doi.org/10.1186/s12877-020-01966-1>.
10. Hayes, K.N.; He, N.; Brown, K.A.; Cheung, A.M.; Juurlink, D.N.; Cadarette, S.M. Over Half of Seniors Who Start Oral Bisphosphonate Therapy Are Exposed for 3 or More Years: Novel Rolling Window Approach and Patterns of Use. *Osteoporos. Int.* **2021**, *32*, 1413–1420, <https://doi.org/10.1007/s00198-020-05794-2>.
 11. Sjølling, A.S.; Christensen, D.H.; Darvalics, B.; Harsløf, T.; Thomsen, R.W.; Langdahl, B. Fracture Rates in Patients Discontinuing Alendronate Treatment in Real Life: A Population-Based Cohort Study. *Osteoporos. Int.* **2021**, *32*, 1103–1115, <https://doi.org/10.1007/s00198-020-05745-x>.
 12. Kim, J.-W.; Yee, J.; Oh, S.-H.; Kim, S.-H.; Kim, S.-J.; Chung, J.-E.; Gwak, H.-S. Machine Learning Approaches for Predicting Bisphosphonate-Related Osteonecrosis in Women with Osteoporosis Using *VEGFA* Gene Polymorphisms. *J. Pers. Med.* **2021**, *11*, 541, <https://doi.org/10.3390/jpm11060541>.
 13. Langdahl, B.L. Overview of treatment approaches to osteoporosis. *Br. J. Pharmacol.* **2021**, *178*, 1891–1906, <https://doi.org/10.1111/bph.15024>.
 14. Kistler-Fischbacher, M.; Weeks, B.K.; Beck, B.R. The effect of exercise intensity on bone in postmenopausal women (part 2): A meta-analysis. *Bone* **2021**, *143*, 115697, <https://doi.org/10.1016/j.bone.2020.115697>.
 15. Åkesson, K.E.; McGuigan, F.E.A. Closing the Osteoporosis Care Gap. *Curr. Osteoporos. Rep.* **2021**, *19*, 58–65, <https://doi.org/10.1007/s11914-020-00644-w>.
 16. Humphrey, W.; Dalke, A.; Schulten, K. VMD: Visual molecular dynamics. *Journal of Molecular Graphics.* **1996**, *14*, 33–38, [https://doi.org/10.1016/0263-7855\(96\)00018-5](https://doi.org/10.1016/0263-7855(96)00018-5).
 17. Tanaka, S.; Tanaka, Y. RANKL as a therapeutic target of rheumatoid arthritis. *J. Bone Miner. Metab.* **2021**, *39*, 106–112, <https://doi.org/10.1007/s00774-020-01159-1>.
 18. Vassaki, M.; Kotoula, C.; Turhanen, P.; Choquesillo-Lazarte, D.; Demadis, K.D. Calcium and Strontium Coordination Polymers as Controlled Delivery Systems of the Anti-Osteoporosis Drug Risedronate and the Augmenting Effect of Solubilizers. *Appl. Sci.* **2021**, *11*, 11383, <https://doi.org/10.3390/app112311383>.
 19. Rauch, L.; Hein, R.; Biedermann, T.; Eyerich, K.; Lauffer, F. Bisphosphonates for the Treatment of Calcinosis Cutis-A Retrospective Single-Center Study. *Biomedicines* **2021**, *9*, 1698, <https://doi.org/10.3390/biomedicines9111698>.
 20. Park, J.; Pandya, V.R.; Ezekiel, S.J.; Berghuis, A.M. Phosphonate and Bisphosphonate Inhibitors of Farnesyl Pyrophosphate Synthases: A Structure-Guided Perspective. *Front Chem.* **2021**, *8*, 612728, <https://doi.org/10.3389/fchem.2020.612728>.
 21. Marocco, C.; Zimatore, G.; Mocini, E.; Fornari, R.; Iolascon, G.; Gallotta, M.C.; Bimonte, V.M.; Baldari, C.; Lenzi, A.; Migliaccio, S. Efficacy of Denosumab Therapy Following Treatment with Bisphosphonates in Women with Osteoporosis: A Cohort Study. *Int. J. Environ. Res. Public Health* **2021**, *18*, 1728, <https://doi.org/10.3390/ijerph18041728>.
 22. Kim, H.J.; Kim, H.J.; Choi, Y.; Bae, M.-K.; Hwang, D.S.; Shin, S.-H.; Lee, J.-Y. Zoledronate Enhances Osteocyte-Mediated Osteoclast Differentiation by IL-6/RANKL Axis. *Int. J. Mol. Sci.* **2019**, *20*, 1467, <https://doi.org/10.3390/ijms20061467>.
 23. Adjei-Sowah, E.; Peng, Y.; Weeks, J.; Jonason, J.H.; de Mesy Bentley, K.L.; Masters, E.; Morita, Y.; Muthukrishnan, G.; Cherian, P.; Hu, X.E.; McKenna, C.E.; Ebetino, F.H.; Sun, S.; Schwarz, E.M.; Xie, C. Development of Bisphosphonate-Conjugated Antibiotics to Overcome Pharmacodynamic Limitations of Local Therapy: Initial Results with Carbamate Linked Sitafloxacin and Tedizolid. *Antibiotics* **2021**, *10*, 732, <https://doi.org/10.3390/antibiotics10060732>.
 24. HyperChem, version 8.0; *Hypercube Inc*: Gainesville, FL, USA, **2007**.
 25. Cohen, G.; and Eisenberg H. Deoxyribonucleate solutions: Sedimentation in a density gradient, partial specific volumes, density and refractive index increments, and preferential interactions. *Biopolymers* **1968**, *6*, 1077–1100, <https://doi.org/10.1002/bip.1968.360060805>.
 26. Beak, P.; Covington J.B.; Smith, S.G., White J.M., and Zeiger J.M., Displacement of protomeric equilibria by self-association: hydroxypyridine-pyridone and mercaptopyridine-thiopyridone isomer pairs. *J. Org. Chem.* **1980**, *45*, 1354–1362, <https://doi.org/10.1021/jo01296a002>.
 27. Kirkwood, J.G. On the Theory of Strong Electrolyte Solutions. *J. Chem. Phys.* **1934**, *2*, 767, <https://doi.org/10.1063/1.1749393>.
 28. Kirkwood J.G. The Dielectric Polarization of Polar Liquids. *J. Chem. Phys.* **1939**, *7*, 911, <https://doi.org/10.1063/1.1750343>.

29. Onsager L. Electric Moments of Molecules in Liquids. *J. Am. Chem. Soc.* **1936**, 58, 1486-1493, <https://doi.org/10.1021/ja01299a050>.
30. Wong M.A., Frisch M.J., and Wiberg K.B., Solvent effects. 1. The mediation of electrostatic effects by solvents. *J. Am. Chem. Soc.* **1991**, 113, 4776-4782, <https://doi.org/10.1021/ja00013a010>.
31. Frisch, M.J.; Trucks, G.W.; Schlegel, H.B.; Scuseria, G.E.; Robb, M.A.; Cheeseman, J.R.; Scalmani, G.; et al. Gaussian, Inc., Wallingford CT. **2009**.
32. Cui Q, Pal T, Xie L: Biomolecular QM/MM Simulations: What Are Some of the “Burning Issues”? *J. Phys. Chem. B* **2021**, 125, 689-702, <https://doi.org/10.1021/acs.jpcc.0c09898>.
33. Elsässer, B.; Goettig, P. Mechanisms of Proteolytic Enzymes and Their Inhibition in QM/MM Studies. *Int. J. Mol. Sci.* **2021**, 22, 3232, <https://doi.org/10.3390/ijms22063232>.
34. Sarasia, E.M.; Afsharnejad, S.; Honarparvar, B.; Mollaamin, F.; Monajjemi, M. Theoretical study of solvent effect on NMR shielding tensors of luciferin derivatives.. *Phys. Chem. Liq.* **2011**, 49, 561-571, <https://doi.org/10.1080/00319101003698992>.
35. Ghalandari, B.; Monajjemi, M.; Mollaamin, F. Theoretical Investigation of Carbon Nanotube Binding to DNA in View of Drug Delivery. *J. Comput. Theor. Nanosci* **2011**, 8, 1212-1219, <https://doi.org/10.1166/jctn.2011.1801>.
36. Monajjemi, M.; Farahani, N.; Mollaamin, F. Thermodynamic study of solvent effects on nanostructures: Phosphatidylserine and phosphatidylinositol membranes. *Phys. Chem. Liq* **2012**, 50, 161-172, <https://doi.org/10.1080/00319104.2010.527842>.
37. Khaleghian, M.; Zahmatkesh, M.; Mollaamin, F.; Monajjemi, M. Investigation of Solvent Effects on Armchair Single-Walled Carbon Nanotubes: A QM/MD Study. *Fuller. Nanotub. Carbon Nanostructures*. **2011**, 19, 251-261, <https://doi.org/10.1080/15363831003721757>.
38. Salo-Ahen, O.M.H.; Alanko, I.; Bhadane, R.; Bonvin, A.M.J.J.; Honorato, R.V.; Hossain, S.; Juffer, A.H.; Kabedev, A.; Lahtela-Kakkonen, M.; Larsen, A.S.; Lescrinier, E.; Marimuthu, P.; Mirza, M.U.; Mustafa, G.; Nunes-Alves, A.; Pantsar, T.; Saadabadi, A.; Singaravelu, K.; Vanmeert, M. Molecular Dynamics Simulations in Drug Discovery and Pharmaceutical Development. *Processes* **2020**, 9, 71, <https://doi.org/10.3390/pr9010071>.
39. Borówko, M. Special Issue on Advances in Molecular Simulation. *Int. J. Mol. Sci.* **2021**, 22, 12484, <https://doi.org/10.3390/ijms222212484>.